Journal of Materials Chemistry B

Accepted Manuscript

ROYAL SOCIETY OF CHEMISTRY

www.rsc.org/materialsB

Cite this: DOI: 10.1039/c0xx00000x

www.rsc.org/xxxxxx

ARTICLE TYPE

Magnetic Fe_3O_4 nanoparticle heaters in smart porous membrane valves†

Aleksandra M. Gajda, Mathias Ulbricht *

Received (in XXX, XXX) Xth XXXXXXXXX 20XX, Accepted Xth XXXXXXXXX 20XX
DOI: 10.1039/b000000x

The application of magnetic nanoparticles (NP) in membrane technology is still very new and combinations of such NP and separation membranes are essentially unexplored. By the integration of NP in polymeric membranes it is possible to create new functionalities based on the synergies of the materials. Here nanoparticle polymer hybrid membranes were created by immobilizing (super)paramagnetic Fe_3O_4 NP on the walls of track-etched polyethylene terephthalate pores and further functionalization with poly(*N*-isopropylacryl-amide) (PNIPAAm). The hybrid system can be controlled via local heat generation by the NP induced by an external high frequency electromagnetic field, i.e., effective membrane pore size can be switched by the magnetic field due to synergy between the nanoparticle functionality and the temperature-responsive properties of PNIPAAm. Analytical characterizations showed a successful and stable NP integration and the feasibility of functionalization with grafted PNIPAAm in presence of immobilized NP on the membrane pore surface. The valve function of the nanoparticle polymer hybrid materials with an external control via a high frequency electromagnetic field was demonstrated in water permeability experiments, but such systems will have significant potential for other applications such as drug release or mass separation.

1 Introduction

Polymeric membranes play a central role in reaction engineering and various separation applications such as water treatment and purification or medical devices. By dedicated further functionalization the membrane properties can be changed or novel separation functions can be created.[1] Stimuli-responsive polymers are popular for surface modification because of their ability to undergo well-defined changes in their properties like shape or volume.[2] The combination of stimuli-responsive polymeric hydrogels can also lead to "smart" membranes where the permeability can be modulated in a reversible manner by changes of, e.g., pH value or temperature.[3] In this field the research on hybrid membranes with immobilised or incorporated nanoparticles is relatively new and many interesting avenues are unexplored; the focus here is on stimuli-responsive membrane barrier properties.

Nanoparticles typically show different properties in comparison to the bulk material. The reduction of the particle diameter can lead to a change of optical, electrical or magnetic behaviour. For instance, by irradiating gold nanoparticles close to the surface plasmon resonance wavelength the light is converted into heat energy. Vankelecom and coworkers used this effect for a hybrid nanofiltration membrane with incorporated gold nanoparticles which is locally heated by irradiation with laser light leading to improved membrane performance (higher flux at unchanged rejection).[4]

Lehrstuhl für Technische Chemie, Universität Duisburg-Essen, Essen,45117, and Center for Nanointegration Duisburg-Essen (CENIDE), Duisburg, 47057, Germany, Fax: +49-201-183-3147, E-mail: mathias.ulbricht@uni-due.de

Iron-based nanoparticles with diameters of up to 100 nm exhibit a unique kind of magnetism called superparamagnetism which enables them to generate heat in an alternating high frequency magnetic field.[5, 6] Magnetic properties are dominated by finite-size and surface effects. The finite-size effect describes the single domain limit and the superparamagnetic limit. Large particles have a multi-domain structure where uniformly aligned electronic spins are separated by walls, due to a balance between the magnetostatic energy and the domain-wall energy. In small particles the energy to create a domain wall is higher than the magnetostatic energy. Therefore the nanoparticle becomes a single magnetic domain where all spins are aligned in the same direction and behave like a giant paramagnetic atom with a fast response to an applied magnetic field. In this case free spin rotation can be induced by an alternating magnetic field. NP have a high percentage of surface atoms, so that surface effects can lead to a decrease of magnetisation. Also, the surface coating can contribute to the magnetic behaviour of NP.[7] Depending on the particle size and the frequency of the magnetic field, the spin rotation (inner magnetisation) competes with the particle rotation (outer magnetisation). The inner magnetisation, the so called Néel relaxation, occurs at high frequencies (> 200 kHz) and the outer magnetisation, called Brownian relaxation, at frequencies below 25 Hz. Which magnetisation type emerges is also influenced by the particle core size and the size of the entire particle.[2, 8] Larger particles with a big core size follow the Néel relaxation because of the giant magnetic moment and heavier weight so that heat is generated. The Brownian relaxation is preferential for small particles which can easily undergo movement. An example for the use of Brownian relaxation are magnetically responsive micromixing membranes which are based on tethering superparamagnetic nanoparticles to grafted hydrophilic and flexible polymer chains; a low frequency rotating magnetic field

caused macroscopic mixing leading to reduced concentration polarization.[9] On the other hand, magnetic heat generating particles are used, for instance, for the stimulation of shape memory polymers,[10] for a controlled drug release in the human body,[11, 12] and as magnetic resonance imaging contrast agent.[13] The research on systems comprising membranes and magnetic particles is widespread in drug delivery, examples are capsules[14, 15] and liposomes.[16] However, the underlying mechanism of these systems is based on thermally disrupting the integrity of a non-porous barrier.

The coupling of (super)paramagnetic nanoparticles and temperature-responsive polymers offers not only new possibilities but also the chance for improvement of already established systems with respect to a better control. Herein we report on the preparation of a track-etched (TE) polyethylene terephthalate (PET) membrane (pore diameter 630 nm) with immobilized Fe_3O_4 nanoparticles (diameter 40 nm) which is further functionalized with the temperature-responsive poly(*N*-isopropylacrylamide) (PNIPAAm). PNIPAAm in water exhibits a lower critical solution temperature (LCST) at 32 °C, i.e., below 32 °C it is swollen and hydrophilic and above 32 °C collapsed and relatively hydrophobic. PET TE membranes functionalized with PNIPAAm had already been shown to behave like valves where pores can be opened or closed when the feed liquid is heated or cooled.[17-19] Synergies of the components of the hybrid material (local nanoparticle heater and temperature-responsive macromolecules) shall be used. Brownian relaxation will not play a role because the nanoparticles are immobilized and the field frequencies are high. Nanoparticles with a diameter of 40 nm were chosen based on results of preliminary experiments with analogous core-shell particles of varied size where NP with a diameter of 15 nm or 25 nm generated less heat under the same magnetic field conditions. Even larger particles were not considered to avoid risk of membrane pore blocking during functionalization. We demonstrate the external control of the effective membrane pore size by an electromagnetic field with high frequencies (Fig. 1a)).

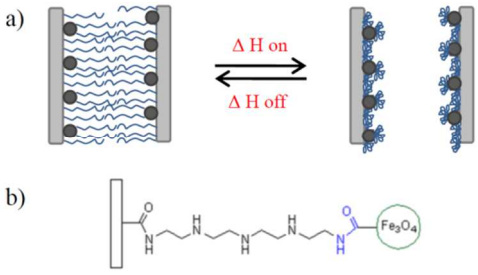

Figure 1 a) Schematic illustration of pore size control via stimulation of superparamagnetic Fe_3O_4 nanoparticles in PNIPAAm functionalized membrane pores in an external magnetic field, b) peptide bond between carboxyl groups on NP surface and prefunctionalized membrane surface.

2 Experimental

2.1 Materials

TE PET membrane with a nominal pore diameter of 400 nm (measured via gas flow/pore dewetting permporometry: 630 nm) and a thickness of 23 µm was purchased from Oxyphen (Germany). Fe_3O_4 NP (40 nm) dispersion (5 g/L) was received from Ocean NanoTech (Arkansas, United States). NIPAAm was obtained from Acros (Belgium) and purified by two times recrystallization after dissolving in boiling n-hexane. 1-Ethyl-3-(3-dimethylaminopropyl)carbodiimide (EDC) and N-hydroxysuccinimide (NHS) were obtained from Sigma Aldrich (Germany) and sodium chloride was from VWR (Germany). A novel cationic macroinitiator, poly(2-methacryloxy-N,N,N-trimethylethanaminiumiodide-co-2-methacryloyloxy-ethyl-4-ethoxy-5-oxo-4,5-diphenylpentanoate) (Fig. 2), was synthesized according to a recent paper[21,†]. For the experiments water was purified with a Milli-Q system (Millipore).

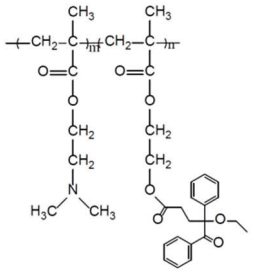

Figure 2 Structure of the cationic and photo-reactive macroinitiator.

2.2 Nanoparticles

The nanoparticles consist of a 40 nm Fe_3O_4 core, a 2 nm monolayer of oleic acid and a 2 nm layer of amphiphilic polymer, providing reactive carboxylic acid groups on the surface. The coating should add approximately 8-10 nm to the core size (supplier data). The organic shells could lead to a reduction of the core particle's magnetic moment and therefore to a lower heat generation effect.[7] The particle size in aqueous dispersion determined via dynamic light scattering (DLS) was 43 nm and the isoelectronic point (IEP) determined via streaming potential measurement was at pH 2.6 (both measured with a Stabisizer instrument; ParticleMetrix, Germany).

2.3 Nanoparticle immobilization

For the nanoparticle immobilization, TE PET membranes were first prefunctionalized with tetraethylenepentamine to generate amine groups at the membrane surface.[17] The nanoparticle immobilization was realized by peptide coupling between the nanoparticle carboxylic acid groups and the amino groups at the membrane surface (Fig. 2b)). Therefore a membrane sample (25 mm diameter) was immersed into 2.3 ml 0.104 g/L Fe_3O_4 dispersion containing 35 mmol/L NaCl. After shaking for 24 h 0.7 ml aqueous solution of 6.2 mg EDC and 5 mg NHS was added; the coupling reaction lasted 4 h. Next, the membrane was washed three times with water and dried over night at 40 °C.

2.4 Photoinitiated graft polymerization of PNIPAAm

Pore surface functionalization with PNIPAAm was achieved via photo-initiated "grafting from".[19] Considering the surface properties of the membranes in that stage, with carboxylic acid

group functionalized NP on the surface (cf. section 2.3), a novel cationic photo-reactive macroinitiator was preadsorbed (20 ml of 1 g/L solution) via filtration (10 min) through the membrane with a syringe pump. Thereafter, the membrane was dried. Further, the membrane was put in a Petri dish between two filter papers and 3 ml 5 % (w/w) NIPAAm water solution were added. The UV irradiation time was 15 min (25 mW/cm^2). After washing the membrane with water it was dried at 40 °C. Control membranes without NP were prepared in an analogous way, but, due to less light scattering, the UV time to obtain membranes with similar degree of grafting was shorter, i.e., 12.5 min. The preparation of specific membranes with and without NP having same water permeability was done by adjusting the UV time considering the relationship between observed degree of grafting and water permeability (cf. section 2.5).

2.5 Membrane characterization

The pore size was determined using the gas flow / pore dewetting method with a PMI capillary flow porometer (Porous Materials, Inc., Ithaca, NY, USA). The gas flow was measured as a function of the trans-membrane pressure, first through a dry membrane and then after wetting the membrane with 1,1,2,3,3,3-hexafluoropropene (surface tension 15,9 dynes/cm). Pore size distribution was calculated using the PMI software. The Fe_3O_4 nanoparticle loading and the degree of grafting (DG) with PNIPAAm were determined by gravimetric analysis; the weight of the membrane was measured in the dry state, before and after immobilization/functionalization. The contact angle was measured using the "sessile drop" method with water at the dry membranes (OCA 15plus; Dataphysics, Germany). Trans-membrane zeta potential measurements were performed using the SurPass electrokinetic analyzer (Anton Paar, Austria). Analyses with membranes equilibrated in a 10^{-3} M KCl solution were started at pH 10.5 and continued by the step-wise addition of HCl down to pH 3. The effect of surface conductivity was considered via an additional measurement with a 0.1 M KCl. The zeta potential was calculated directly by the instrument software (VisioLab) using the Fairbrother-Mastin method based on the Helmholtz-Smoluchowski equation. For scanning electron microscopy (SEM) images, the membranes were sputtered with Au (Sputter Coater K550; Emitech). The analyses were performed using an ESEM Quanta 400 (FEG, Czech Republic) which also has an additional tool energy dispersive X-ray (EDX) analyses. For determination of Fe content on the membranes atomic absorption spectroscopy was performed (instrument M series; Thermo Electron Cooperation). Therefore the membranes were dissolved and the Fe NP open via 6 M HCl. Water flux measurements were performed using a self-constructed dead-end filtration cell with 1 ml volume and 3.46 cm^2 active membrane area. The trans-membrane pressure was adjusted by the height of a water reservoir above the membrane. The mass of permeate as function of time was continuously measured gravimetrically, and the feed reservoir was refilled synchronous with collection of permeate.

2.6 Electromagnetic field experiments

The electromagnetic field experiments were performed using a high frequency electromagnetic field generator (TrueHeat HF 5000; Hüttinger). To analyse the heating effects by the NP, 1 ml of a 0.25 mg/ml dispersion in an Eppendorf tube was exposed for 1.5 and 5 min to the electromagnetic field. The narrow inductor (2.7 cm high; 1.7 cm wide) covered the whole vessel. Immediately before and after the incubation the temperature was measured with a contact thermometer (Ahlborn). Variations of current and frequency were performed. Analogous experiments were performed with pure water. The membrane flux measurements with electromagnetic field were done like described in section 2.5. The inductor was a sandwich coil, consisting of two coils (one above the other). The filtration cell was placed between both coils which generate the electromagnetic field. The operating conditions were adjusted at a frequency of 746 kHz, a current of 15.6 A and a voltage of 712 V so that a power of 368 kW and an electromagnetic field of about 1150 A/m results. The field strength for the particular inductor geometry had been estimated by simulations. Typically, one experiment lasted for 35 min. The electromagnetic field was switched on for 20 min. For the first 5 and the last 10 min the flux measurement was done without magnetic field. A scheme and two photographs of the filtration set-up can be found in Electronic Supplementary Information.†

3 Results and discussion

3.1 Nanoparticle immobilization

First experiments for NP immobilization were done with the NP dispersion without adding salt. The NP loading of the still colourless membrane was 0.25 % and SEM images showed a low NP density at the outer membrane surface and no NP in the pores. To resolve this problem, a defined concentration of NaCl was added to the NP dispersion to reduce the electrostatic interactions between the negatively charged NP (due to surface carboxylic acid groups; IEP = 2.6; cf. section 2.2).

After the nanoparticle immobilization with added 35 mmol/L NaCl the membranes turned deep-brown; images can be found in Electronic Supplementary Information.† The nanoparticle loading was determined by gravimetric analysis, yielding a total content of nanoparticles in the membrane of 2.42 % (w/w). The Fe content was calculated by subtracting the masses of inorganic oxygen according to the Fe_3O_4 stoichiometry and of the polymer shell, ignoring the unknown oxygen content of the polymer. The organic fraction of the core-shell particles had been determined via elemental analysis (H: 0.76 % N: 0.04 %, C: 5.08 %; w/w). The result of this estimation of iron content was 1.68 % (w/w). The iron content determined via atomic absorption spectroscopy was 1.54 % (w/w). This is in the same range but somewhat lower than the iron content calculated from gravimetry and nanoparticle composition. One reason is that the organic oxygen content had been neglected in the calculation based on gravimetry (cf. above). Immobilization experiments with higher salt concentrations show that an adjusted NaCl concentration is necessary for a high and uniformly distributed NP loading. For example, no NP in the pores and an iron content determined gravimetrically of 0.73 % (w/w) were obtained at 50 mmol/L NaCl. The reason for this much less efficient immobilization at a higher salt concentration

is still unexplained. All further preparations were done using the protocol with NP dispersions containing 35 mmol/L NaCl.

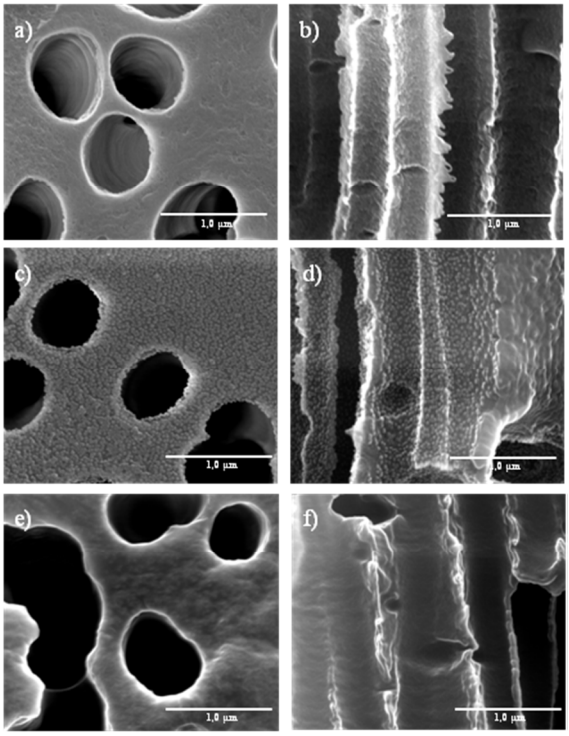

Figure 3 SEM images of: a) the aminated PET membrane outer surface; b) the aminated PET membrane cross-section; c) the nanoparticle immobilized PET membrane outer surface; d) the nanoparticle immobilized PET membrane cross-section; e) the PET-NP-g-PNIPAAm membrane outer surface; f) the PET-NP-g-PNIPAAm membrane cross-section; all at a 100,000 fold magnification.

SEM was used to confirm nanoparticle immobilisation at the membrane surface and in the pores. Figure 3 presents images at 100,000 fold magnification. Fig. 3a) shows the aminated PET membrane outer surface and Fig. 3b) the cross-section in the middle of the 22 µm thick membrane. In both cases a relatively smooth polymer surface and cylindrical pores can be seen. Fig. 3c) and 3d) show the membrane outer surface and the middle part of the cross-section of the membrane, all covered with nanoparticles. The topographic features are clearly different from the PET base membrane because of bright grey spherical objects. EDX analyses reveal significant iron peaks which are not observed for the precursor membranes. The nanoparticles are uniformly distributed across the outer and inner membrane surface and no aggregates are observed. That the immobilization is stable was observed in washing tests; the nanoparticle content remained constant after 45 minutes flow-through washing with water in a filtration cell. All observations seem to confirm the nanoparticle coupling at the membrane surface by peptide bonds and not by physical adsorption. The particle density seemed to be high, and considering that the polymeric shell is not visible in SEM, monolayer coverage of the PET surface seems to have been obtained.

Table 1: Water contact angle (CA) and water flux at a trans-membrane pressure of 2100 Pa at 25 °C and 45 °C at each stage of membrane functionalization (fluxes had been measured with dried membranes, i.e., without pre-wetting the pores with ethanol; only for PET-NP the measured flux was influenced by pre-wetting; cf. text).

Membrane	CA (°)	flux at 25 °C (L/m^{2}h)	flux at 45 °C (L/m^{2}h)
aminated PET	46.0	833.2	1004.9
PET-NP	139.1	0	
PET-NP-macroinitiator	115.2	559.0	
PET-NP-g-PNIPAAm	95.7	41.6	355.8
PET-g-PNIPAAm	78.9	55.5	348.5

To characterize the change in surface properties, sessile water drop contact angle and zeta potential measurements were done. The CA of the aminated PET membrane was 46°. After NP immobilisation the CA increased to 139° (Table 1). This shows that the membrane is hydrophobic despite of the oleic acid shell of the nanoparticles and, hence, carboxylic acid groups at the surface. The CA of a dry thin nanoparticle layer on a glass substrate was also measured for comparison and a value of 90.2° was found. The surprising finding for the membranes might therefore be because of a partial reorientation of the oleic acid on the nanoparticle surface upon drying and the combined macro- and nanoscale roughness of the nanoparticle coated membranes (cf. Fig. 3c); the latter making the surface appear super-hydrophobic.

Water flux measurements confirmed an increase of membrane hydrophobicity due to the NP coating, i.e. flux of a not pre-wetted membrane was zero. The flux increased to almost the same value as for an aminated membrane (833 L/m^{2}h; cf. Table 1) after pre-wetting the pores with ethanol (817 L/m^{2}h). Despite of a water CA of 115°, the not pre-wetted PET-NP-macroinitiator membrane showed a flux of about 550 L/m^{2}h. Because the surface hydrophobicity is lower than of the PET-NP membrane the pores can be wetted by water leading to water flow without pre-wetting.

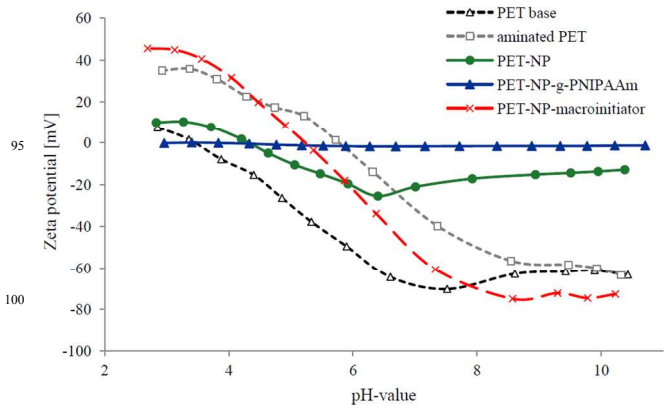

Figure 4 Transmembrane zeta potential versus pH for base, aminated, nanoparticle immobilized, macroinitiator immobilized and thereafter PNIPAAm functionalized membranes.

The trans-membrane zeta potential of initial, nanoparticle

immobilized and PNIPAAm functionalized membranes, yielding information about the charge of the pore surface, is shown in Fig. 4. The PET base membrane has carboxylic acid groups at the surface, so that the charge was clearly negative down to pH 3.5 (isoelectric point, IEP). The IEP of the aminated PET membrane was at pH 5.8 and the membrane had a positive zeta potential of 35 mV at the lowest studied pH value. The IEP of the nanoparticle immobilized membrane (pH 4.2) was close to that of the PET base membrane because of the dense nanoparticle layer exposing some carboxylic acid groups at surface. A lower IEP of 2.6 was observed for the nanoparticles in aqueous dispersion (cf. section 2.2). Considering also the contact angle results (cf. Table 1), the polymeric shell of the nanoparticles seems to have some flexibility to allow re-orientation, and, hence, different surface properties in dry and wet state.

3.2 PNIPAAm graft polymerization

The macroinitiator (cf. Fig. 2) should adsorb electrostatically at the carboxylic acid groups, exposed by the NP which are immobilized of the membrane surface. Upon UV irradiation the benzoin side group of the macroinitiator is cleaved, and surface confined starter radicals for a radical polymerization are created.

The PNIPAAm functionalization was measured via gravimetric analysis yielding the degree of graft functionalization (DG). The DG values of the further studied PNIPAAm grafted aminated PET membranes were about 0.86 μg/cm^2 and those of the PNIPAAm grafted membrane with immobilized nanoparticles were about 1.65 μg/cm^2. These membranes were selected because of their similar water flux at 25 °C and 45 °C and their similar switchability of flux (Table 1). That a higher DG is required to obtain the same degree of pore narrowing by the grafted polymer layer may be explained by the rougher surface of the nanoparticle immobilized membranes (cf. section 3.1), so that a larger fraction of the PNIPAAm is physically cross-linked and, hence, contributes less to the swelling of the layer.

SEM images indicate a smoother outer and inner membrane surface after functionalization with PNIPAAm. The NP layer is completely covered with the temperature-responsive polymer so that no NP can be observed anymore (Fig. 3 e) and f)).

The contact angle changed after adsorption of the macroinitiator from 139.1° (PET-NP) to 115.2°. Thus a hydrophobicity change of the surface is clearly seen and can be related to the introduction of cationic groups on the surface (note that not all of these groups on the polymer chain may be associated with carboxylic acid groups on the membrane surface[21]). After functionalization with PNIPAAm the CA was 95.6°. For comparison, a membrane only functionalized with PNIPAAm (without nanoparticles) had a CA of 78.9°. Hence, the functionalization with grafted PNIPAAm had been confirmed by the large reduction of CA but the surface topography of the NP polymer hybrid membrane surface in dry state is more complex than that of the just polymer grafted membrane. Overall the CA data show a large alteration of the membrane surface properties in each stage of the functionalization sequence (Table 1).

It was expected that the zeta potential should shift to higher pH values due to cationic groups after macroinitiator adsorption. The absolute zeta potential did not show this trend very clearly but the IEP at pH 5.2 was obviously significantly higher than that of the membrane covered with NP. This can be related to the fact that most but not all cationic groups were associated with carboxylic acid groups on the membrane surface. The nanoparticle immobilized and then with PNIPAAm functionalized membrane showed only very low absolute values of the zeta potential in the entire pH range. This is expected for a surface completely covered by a neutral PNIPAAm hydrogel layer.[18]

The permeability values in Table 1 show a clear switchability due to the temperature-responsive properties of PNIPAAm at different feed temperatures for both functionalized membranes. The pore size of the PNIPAAm functionalized membranes at 25 °C was estimated from water permeability via Hagen-Poiseuille law[22] to be about 290 nm, and at a temperature above the LCST of PNIPAAm the pore diameter is much larger, e.g., about 550 nm at 45°C. This result shows that both membranes behave like valves where the pore size can be controlled by the feed temperature.

3.3 Electromagnetic field experiments

To adjust the best conditions for the largest heat generation and the lowest "back ground" water heating, experiments with 0.25 g/L Fe_3O_4 nanoparticle dispersions were done. The frequency depends on the capacitor and the adjusted current. The current was regulated manually, and the voltage and power were adjusted and calculated by the generator. Table 2 shows the temperature difference between pure water and the Fe_3O_4 nanoparticle dispersions at different frequencies and currents. The largest heat generation was recorded at a current of 17.5 A and a frequency of 720 kHz. At all current settings the heating at > 700 kHz was more effective that at < 520 kHz. To obtain a big difference in heat generation between NP and water, but to have a limit for the water heat generation, a frequency of 746 kHz, a current of 15.6 A and a voltage of 712 V so that a power of 368 kW results were determined to be best suited for water flux experiments. Under those conditions the temperature difference between 1 ml pure water and 1 ml nanoparticle dispersion was 9.1 K after 1.5 minutes and 17.7 K after 5 minutes in the electromagnetic field. A nonspecific heating of pure water of 5.4 K after 1.5 minutes and 10.9 K after 5 minutes in the electromagnetic field occurred. Such effect was observed also in previous studies due to the thermal loss in the environment of the inductor coil.[21, 22] Under the used conditions, the inductor coil stayed cold so that we assume that the nonspecific water heating in the electromagnetic field occurs by inductive heating due to current induced in the fluid (water) having relatively good electric conductivity.

Table 2: Temperature difference between pure water and 0.25 g/L Fe_3O_4 nanoparticle dispersions at different frequencies (f) and current at a start temperature range of 21.0 – 25.6 °C

current (A)	f < 520 kHz [K]		f > 700 kHz [K]	
	1.5 min	5 min	1.5 min	5 min
23.5	7.5	13.8	10.9	20.4
20.0	6.6	14.6	11.2	17.0
17.5	7.3	13.4	13.5	20.3
15.6	7.5	14.9	9.1	17.7

To demonstrate an external pore size control, water flux measurements at a pressure of 2100 Pa were performed in the high frequency electromagnetic field at the same conditions. Therefore, the filtration cell was put between two inductor coils which generate the electromagnetic field (cf. section 2.6). The operating conditions were adjusted at a frequency of 746 kHz and a current of 15.6 A (i.e., a power of 368 kW; cf. above).

In the first 5 minutes the flux measurements were done without magnetic field, afterwards the electromagnetic field was turned on for 20 minutes and then turned off again to measure flux after the magnetic excitation (Figure 5). The flux after 5 minutes without electromagnetic field was almost the same for the PNIPAAm functionalized membranes without and with immobilized nanoparticles (cf. Table 1). After turning on the electromagnetic field the flux increased slowly and a maximum value of about 150 L/m^{2}h was reached for the PET-g-PNIPAAm membrane. The increase in permeability was caused by the nonspecific heating of water as also observed in the preliminary experiments with water in test tubes (cf. above). The PET-NP-g-PNIPAAm membrane reached a higher absolute flux value of about 240 L/m^{2}h with a higher initial slope after switching on the electromagnetic field. The higher permeability increase results from nanoparticle heating in addition to "back-ground" water heating, both triggered by the external excitation. After turning off the electromagnetic field, the permeability decreased to the initial values of both membranes; so reversibility of switching was demonstrated.

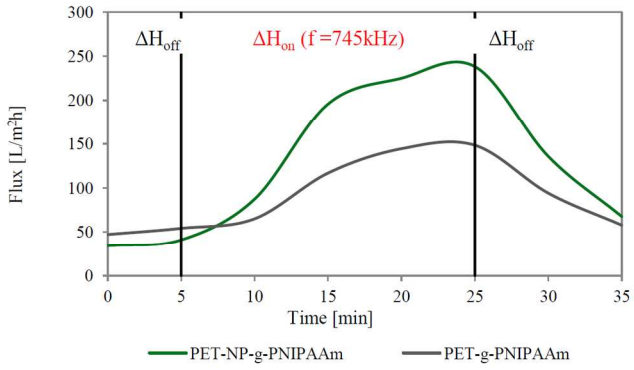

Figure 5 Water flux through PNIPAAm functionalized membranes as function of time without and with external electromagnetic field at a frequency of 745 kHz and a trans-membrane pressure of 2100 Pa and a feed temperature of 22 °C.

By comparing the flux value obtained for the same membrane where the feed had been preheated (356 L/m^{2}h; cf. Table 1), the flux did not reach the same value in the electromagnetic field. It must be considered that an interplay of the magnetically induced heating within the pores and the convective cooling by the increasing water flux through the pores will occur. Apparently, this did not allow the complete PNIPAAm collapse and consequently not achieving the maximum permeability value like via preheating the whole feed.

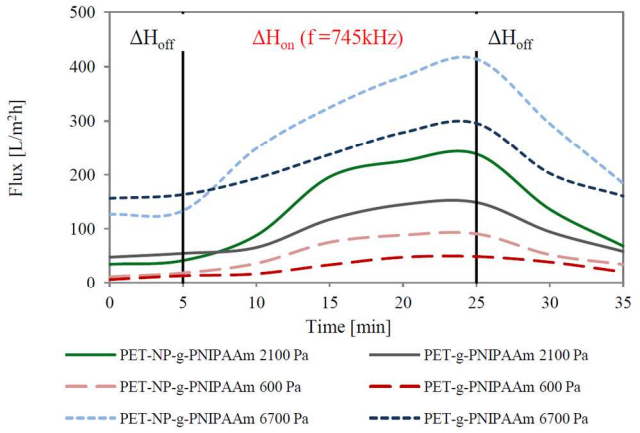

Figure 6 Water flux through PNIPAAm functionalized membranes as function of time without and with external electromagnetic field at a frequency of 745 kHz at different transmembrane pressures and a feed temperature of 22 °C.

To get more information about the competing local heating and convective cooling effects, flux experiments with external electromagnetic field at different trans-membrane pressures and, hence, different initial water fluxes were performed. By decreasing the pressure the convective flux should decrease and as consequence the effective membrane heating increase. Thus the membrane temperature should reach a higher value and a more effective PNIPAAm collapse would be possible. Figure 6 shows the fluxes for PNIPAAm functionalized membranes at different pressures. A two times higher initial water flux was observed at 6700 Pa compared to 2100 Pa and the flux at 600 Pa was less than half of the value at 2100 Pa. The flux did not correlate linearly with the pressure due to a possible pressure loss in the filtration cell at higher nominal trans-membrane pressures. More importantly, the expectations regarding the stimuli-responsive behaviour response were fulfilled qualitatively. The maximum flux difference between the PET-g-PNIPAAm and the PET-NP-g-PNIPAAm membrane at the same pressure increased with decrease of trans-membrane pressure. The flux difference at 6700 Pa was 28.5 %. For 2100 Pa a flux difference of 37.7 % and for 600 Pa a difference of 46.3 % were obtained. The reason for this effect can be described by a more effective convective cooling by the feed at higher flux through membranes, leading to lower temperature increase in the same time (note that for the higher fluxes, a stationary state had not yet been achieved; cf. Figure 6).

In Figure 7 the results of a long time flux experiment with external electromagnetic field at 600 Pa trans-membrane pressure are shown. The electromagnetic field was turned on for 55 minutes and then turned off. The flux did not increase further after about 20 minutes in the electromagnetic field. The flux in this state was significantly higher for the membrane with integrated nanoparticles. For both PET-g-PNIPAAm and PET-NP-g-PNIPAAm a small oscillation of flux was observed. Qualitatively, this dynamic instability of the stationary state is related to the competing effects of heat generation in the pores and convective cooling by flow through the pores.

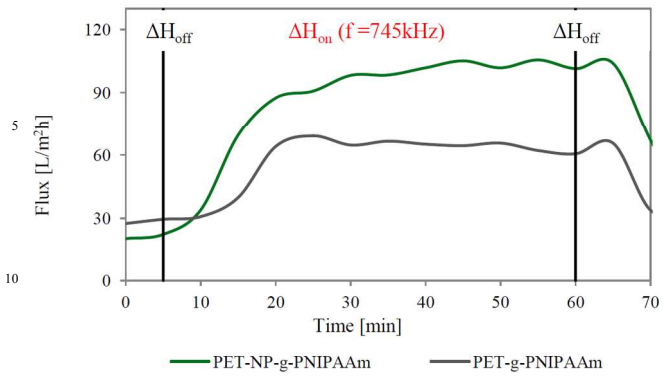

Figure 7 Long time water flux experiments with PNIPAAm functionalized membranes as function without and with external electromagnetic field at a frequency of 745 kHz and a trans-membrane pressure of 600 Pa and a feed temperature of 22 °C.

3.4 Heat generation in the membrane pores by external magnetic field and influences on responsive valve function

An important feature of the developed hybrid system is the amount of heat generation by the NP and its effects on a "smart" valve function.

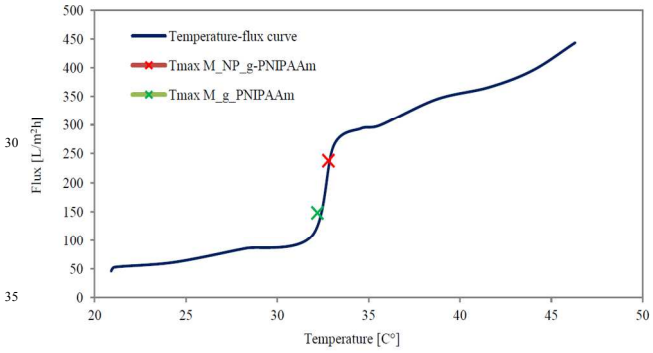

Figure 8 Water flux vs. temperature curve for PNIPAAm functionalised membrane by heating the feed at a trans-membrane pressure of 2100 Pa

Figure 8 shows the water flux as function of temperature obtained by heating the feed, revealing a very sharp increase of flux in a relatively narrow range around the LCST of 32-33°. Below and above that range, the increase of flow with increasing temperature is much less pronounced, and it is to a large extent due to the decreasing viscosity of the water as also seen for the water flux through the aminated TE PET membrane without temperature-responsive polymer (cf. Table 1).[18] The amount of heat generated by the NP will have influence on the temperature in the pore in the stationary state with field excitation (magnitude of switching effect) and also on the time to reach the LCST in the membrane pore thus inducing the PNIPAAm collaps (response time for switching). Using the data from Figure 5 where the filtration had been done at the same trans-membrane pressure, the temperature in the membrane pores reached after 20 minutes in the magnetic field was estimated from the respective flux values. The temperature difference between the PET-g-PNIPAAm membrane (32.4 °C; deduced from a flux of 150 L/m^{2}h) and PET-NP-g-PNIPAAm (32.9 °C, reduced from a flux of 240 L/m^{2}h) is about 0.5 K. This illustrates again the specific heating effect due to the pore-immobilized superparamagnetic nanoparticles. However, the membranes with nanoparticles experienced also a much stronger convective cooling.

An attempt had been made to use the data obtained for the NP dispersions and the information on NP loading of the membranes to quantitatively analyse the effects leading to the experimental observations. The advantage of track-etched membranes is their well-defined pore structure so that reliable information about the pore geometry and pore density is available. The known data for the membrane used in this study are number of pores per membrane sample with a diameter of 25 cm ($N_{pores} = 2.16*10^8$) and volume per pore with diameter of 630 nm and a thickness of 23 µm (cf. section 2.1) corresponding to the mass of water per pore ($m_{H2O/pore} = 6.86*10^{-16}$ m^3). The number of NP in one membrane pore ($N_{NP/pore}$) can then be calculated from the mass of one NP ($m_{NP} = 1.74*10^{-16}$ g) and the gravimetrically determined total mass of NP in the membrane ($m_{NP/membr}$; Eq. 1).

$$(1) \qquad N_{NP/pore} = (m_{NP/membr} / m_{NP}) / N_{pores}$$

With $m_{NP/membr}$ = 0.19 mg (from 2.42 wt%; cf. section 3.1), a value of $N_{NP/pore}$ = 6786 was obtained.

The number of NP in 1 ml 0.25 g/L dispersion was calculated also using m_{NP}; the result is $N_{NP/disp} = 2.0*10^{12}$. With this number, the data for temperature increase by excitation of the NP dispersion with a known NP mass (cf. Table 2) were used to calculate the heat flow into the water ($\dot{Q}_{disp}$; Eq. 2) and from that also the heat flow induced by one NP ($\dot{Q}_{NP}$; Eq. 3).

$$(2) \qquad \dot{Q}_{disp} = (\Delta T * m_{NP/disp} * c_w) / t$$

$$(3) \qquad \dot{Q}_{NP} = \dot{Q}_{disp.} / N_{NP,disp}$$

ΔT = temperature difference within time with field (K)
$m_{NP/disp}$ = mass of NP in dispersion (g)
c_w = specific heat capacity of water at 20 °C (J/kg K)
t = time with field (s)

Using the data for 1.5 minutes at 15.6 A and > 700 kHz and assuming constant heat capacity, the heat flow for one NP ($\dot{Q}_{NP}$) amounts to $2.1*10^{-13}$ J/s (see Table 3). Further, the heat generation per pore ($\dot{Q}_{pore}$) was obtained from the number of NP in one pore ($N_{NP/pore}$) and $\dot{Q}_{NP}$ (Table 3). With the value for $\dot{Q}_{pore}$, the time (Δt) to reach 32 °C in the pore starting with a temperature of 22°C (ΔT = 10 K) without convective cooling was calculated via equation 4.

$$(4) \quad \Delta t = (\Delta T * m_{H2O/pore} * c_w) / \dot{Q}_{pore}$$

All calculations were also done for heat generation of pure water, and the specific effects by the nanoparticles were the difference between that data and the ones for membranes with NP (Table 3).

Table 3: Heat flow and time to reach 32 °C in one pore starting with a temperature of 22°C without convective flux, for pores with immobilized NP and water as well as pore with only water, and the specific effect of nanoparticles (based on data from Table 2 for 1.5 minutes).

	NP+H_2O	only H_2O	NP
$\dot{Q}_{disp}$ (J/s)	0.70	0.25	0.42
$\dot{Q}_{NP}$ (J/s)	$3.4*10^{-13}$	$1.2*10^{-13}$	$2.1*10^{-13}$
$\dot{Q}_{pore}$ (J/s)	$2.3*10^{-9}$	$8.4*10^{-10}$	$1.4*10^{-9}$
Δt to 32 °C (s)	12	34	20

The calculated values of the heat flow per pore ($\dot{Q}_{pore}$) reveal almost two times more heat generation by NP compared with pure water. The largest heat generation is obtained by combining NP and water, the fastest time (12 s) to reach 32 °C in the pores without convective cooling is obtained by the system comprising immobilized NP and water in the pore. Without NP, the time to reach LCST would be almost three times longer (34 s). In the membrane experiments, the observed onset times for flux increase (i.e., the time where PNIPPAm chains start to collaps) were significantly, by one order of magnitude, longer. More important, the onset times with the NP loaded membranes (9 min) were almost two times shorter compared to the one without NP (16 min; cf. Figure 7). It must be noted that the fluxes were measured with a macroscopic system having characteristic volumes in the cell outside the membrane (1 mL) which are much larger than the total pore volume ($1.48*10^{-4}$ mL); this will obviously cause a significant delay in response. On the other hand, it had been demonstrated that the intrinsic swelling/deswelling times of PNIPAAm layers with a thickness in the range of 100 nm (as also used in this study) are in the order of several microseconds.[23] Therefore, the macromolecular part of the smart valve will not impose critical limitations with respect to response time.

An estimate for the influence of convective cooling onto prolonging the onset time can help to further rationalize the quantitative effects in the system. The heat flow due to convection in one pore ($\dot{Q}_{conv/pore}$) can be estimated using Eq. 5.

$$(5) \quad \dot{Q}_{conv/pore} = \dot{m}_{H2O/pore} * c_{wH2O} * \Delta T$$

$\dot{m}_{H2O/pore}$ = mass flow through one pore (kg/s)
ΔT = temperature difference between feed and pore (K)

The mass flow had been calculated from the measured water fluxes and number of pores per membrane (N_{pores}; cf. above). Table 4 presents data for two cases, either directly after switching on the electromagnetic field and at 32°C in the pore; the feed temperature is in both cases 22°C.

According to this estimation, the effect of convective cooling is relatively small after switching on the field, about 11% compared to the non-specific heating of pure water (ratio of heating vs. cooling = 8.9), and less than 3% for the combined effects of NP-specific and non-specific heating (ratio 30). Note that the ratio between heating and cooling would be still much larger if the membrane with immobilized NP would have been operated at the same initial flux as the control membrane, i.e., $\dot{Q}_{pore} / \dot{Q}_{conv/pore} = 24.1$ at 50 L/m^{2}h. Hence, the much larger response time observed experimentally than estimated (cf. Table 3) cannot be explained by convection alone. On the other hand, one can see that in the range of LCST, the estimated effects of convective cooling ($\dot{Q}_{conv/pore}$) are larger than the (also estimated) pore heating induced by the electromagnetic field ($\dot{Q}_{pore}$); all ratios are <1. This result could explain why stationary fluxes are obtained which are significantly lower than fluxes obtained with warm feed (e.g., 45°C, cf. Table 1). However, a complete quantitative description should give reasonable agreement for both cases. Therefore, we must conclude that the used estimations give at the best a semi-quantitative description of the stimuli-responsive valve system.

Table 4: Heat flow into one pore induced by the electromagnetic field and out of one pore via water flow (convective cooling) for two cases, i.e., temperature differences between feed and pore (calculated with water fluxes at 22°C from Figure 5: NP+H_2O: 40 L/m^{2}h; H_2O: 50 L/m^{2}h, and an increase of flux from 22°C to 32°C by a factor of 5.8; cf. Figure 8).

	NP+H_2O	only H_2O	NP
$\dot{Q}_{pore}$ (J/s)	$2.3*10^{-9}$	$8.4*10^{-10}$	$1.4*10^{-9}$
$\dot{Q}_{conv,pore}$ (J/s), ΔT = 1 K	$7.6*10^{-11}$	$9.5*10^{-11}$	$7.6*10^{-11}$
→ ratio $\dot{Q}_{pore} / \dot{Q}_{conv/pore}$	30.0	8.9	19.0
$\dot{Q}_{conv,pore}$ (J/s), ΔT = 10 K	$4.4*10^{-9}$	$5.5*10^{-9}$	$4.4*10^{-9}$
→ ratio $\dot{Q}_{pore} / \dot{Q}_{conv/pore}$	0.52	0.15	0.33

There are many problems with these estimations which should step-by-step be solved in further experiments and model development. In addition to the need for improvement of the filtration cell, which will reduce the time delay for observation of flux increase (cf. above), there are several other points. First, the assumptions about pore geometry and nanoparticle loading per pore will introduce an error what is not known at this stage. Second, the estimation of heat flow per nanoparticle from the separate batch experiments is certainly not very accurate, especially because of the different inductor geometry and the insufficient thermal isolation. Third, the non-specific heating of water can also take place before and after the membrane. However, the much higher effects seen for membranes with superparamagnetic nanoparticles are proof that this is only a possible additional effect. Forth, the assumption of no (axial and radial) temperature gradients within the pore during the instationary period is not corresponding to reality; consequences are gradients in PNIPAAm deswelling along the pore but also in radial direction. With the contribution of non-specific heating of the water in the volume of the pore in addition to the specific heating by the nanoparticles on the pore wall, a realistic description of the microscopic behaviour of the polymer layer on the pore wall becomes very challenging. Fifth, the complex global response of the system as function of temperature (cf. Fig. 8) is also only partially considered in the estimations.

Nevertheless, the feasibility of the novel smart valve system based on a polymer-nanoparticle hybrid material had been clearly demonstrated. The non-specific heating of the water had been identified as a complication. However, it can be clearly seen that the heat generation of water in addition to the one by the NP can also be taken as an advantage for the hybrid membrane valve system for a faster and more effective control of the membrane

pore size via the external electromagnetic field.

4 Conclusions

Immobilization of (super)paramagnetic Fe_3O_4 nanoparticles via a peptide bond between carboxylic acid groups of the NP shell and amino groups on the pre-functionalized PET membrane surface allows the preparation of a uniformly distributed and stable NP layer across the outer and inner membrane surface. An additional functionalization with the temperature-responsive polymer PNIPAAm is possible by pre-adsorbing a cationic macroinitiator and subsequent photo-initiated graft copolymerization. Using this strategy, we have fabricated stimuli-responsive polymer-nanoparticle hybrid membranes. An effective switching of the water flux by "remote control" (electromagnetic field "on" vs. "off") could be achieved. The magnitude of the response was a function of the trans-membrane pressure what can be explained by the interplay of heating in the pores and convective cooling by flow through the pores. This gives also rise to dynamic instabilities, small flux oscillations, in the range of stationary state. Besides the NP-specific heat generation, a non-specific heating of the water had been observed. All quantitative data from membrane characterization had been used for an estimation of the effective time to reach the LCST of PNIPAAm (32 °C) starting with 22 °C feed temperature: This should be possible within 12 sec. Observed response times were by one order of magnitude longer, at least partially due to the not optimized system around the membrane. To obtain a stronger membrane pore size switching effect by "remote control", more and larger nanoparticles can be immobilised in the membrane. In further experiments also the PNIPAAm chain length and grafting density as well as the membrane pore size will be varied. Influences of initial flow rate via trans-membrane pressure onto the efficiency of the valve effect had already been identified. However, also the feed temperature can be increased to shorten the response time and increase the magnitude of the response under otherwise identical conditions. The hybrid membranes presented in this proof-of-concept study show a remote controlled change of effective pore size between about 290 nm without and > 400 nm with electromagnetic field excitation; i.e. in the microfiltration range. However, the extension of the work to pore-surface functionalized or pore-filled thermo-responsive capillary pore membranes where barrier properties in the ultrafiltration range are switched reversibly[24,25] is also possible and currently studied. All the possible design parameters make the novel system very promising for further exploration, for example toward smart drug release or mass separation systems.

Acknowledgements

The contribution of Kristina Evdoshenko, student at UDE, who performed experiments during the work for her Bachelor Thesis is gratefully acknowledged. The authors thank also Prof. Dr. Daniel Erni and David Schäfer, Department of Electrical Engineering, UDE, for the simulation of the electromagnetic field.

Electronic Supplementary Information

Protocol for synthesis of cationic and photoreactive macroinitiator; scheme and two photographs of the set-up used for the filtration experiments with external stimulation of the membrane by high frequency electromagnetic field; optical images of membranes before and after nanoparticle immobilization.

References

1. M. Ulbricht, *Polymer*, 2006, **47**, 2217-2262.
2. T. Neuberger, B. Schöpf, H. Hofmann, M. Hofmann, *Journal of Magnetism and Magnetic Materials*, 2005, **293**, 483-496.
3. N. Adrus, Q. Yang, F. Tomicki, M. Ulbricht, *Journal of Materials Chemistry*, 2011, **21**, 2783-2811.
4. K. Vanherck, I. Vankelecom and T. Verbiest, *Journal of Membrane Science*, 2011, **373**, 5-13.
5. D. L. Huber, *Small*, 2005, **1**, 482-501.
6. K. M. Krishnan, *IEEE Transactions on Magnetics*, 2010, **46**, 2523-2558.
7. A. H. Lu, E. L. Salabas and F. Schüth, *Angewandte Chemie International Edition*, 2007, **46**, 1222-1244.
8. V. S. Kalambur, B. Han, B. E. Hammer, T. W. Shield and J. C. Bischof, *Nanotechnology*, 2005, **16**, 1221-1233.
9. H. H. Himstedt, Q. Yang, L. P. Dasi, X. Qian, S. R. Wickramasinghe and M. Ulbricht, *Langmuir*, 2011, **27**, 5574-5581.
10. R. Mohr, K. Kratz, T. Weigel, M. Lucka-Gabor, M. Moneke and A. Lendlein, *Proceedings of the National Academy of Sciences of the United States of America*, 2006, **103**, 3540-3545.
11. S. H. Hu, T. Y. Liu, D. M. Liu and S. Y. Chen, *Macromolecules*, 2007, **40**, 6786-6788.
12. E. Ruiz-Hernández, A. Baeza and M. A. Vallet-Regí, *ACS Nano*, 2011, **5**, 1259-1266.
13. R. C. Stoldt, B. A. Larse, K. M. Hurst and R. W. Ashurst, *Journal of Material Research*, 2012, **27**, 1846-1852.
14. S. Lecommandoux, O. Sandre, F. Chécot and R. Perzynski, *Progress in Solid State Chemistry*, 2006, **34**, 171-179.
15. X. Ju, J. Wei, R. Xie and L. Chu, *Patent application,* CN 102258498 A 20111130, 2011.
16. E. Amstad, J. Kohlbrecher, E. Müller, T. Schweizer, M. Textor and E. Reimhult, *Nano Letters*, 2011, **11**, 1664-1670.
17. C. Geismann, and M. Ulbricht, *Macromolecular Chemistry and Physics*, 2005, **206**, 268-281.
18. C. Geismann, A. Yaroshchuk and M. Ulbricht, *Langmuir*, 2006, **23**, 76-83.
19. A. Friebe and M. Ulbricht, *Macromolecules*, 2009, **42**, 1838-1848.
20. J. Lei, and M. Ulbricht, *Journal of Membrane Science,* in revision.
21. A. Chalkidou, K. Simeonidis, M. Angelakeris, T. Samaras, C. Martinez-Boubeta, L. Balcells, K. Papazisis, C. Dendrinou-Samara and O. Kalogirou, *Journal of Magnetism and Magnetic Materials*, 2011, **323**, 775-780.
22. B. Paya, *Przeglod Electroniczny*, 2008, pp. 129-133.
23. C. A. Naini, S. Franzka, S. Frost, M. Ulbricht and N. Hartmann, *Angewandte Chemie International Edition*, 2011, **50**, 4513-4516.
24. S. Frost, M. Ulbricht, *J. Membr. Sci.* 2013, **448**, 1-11.
25. N. Adrus, M. Ulbricht, *J. Mater. Chem.* 2012, **22**, 3088-3098